Self-Consistent Simulation of Opto-Electronic Circuits Using a Modified Nodal Analysis Formulation

Pavan Gunupudi, *Member, IEEE*, Tom Smy, Jackson Klein, and Z. Jan Jakubczyk

***Abstract*—This paper addresses the need for self-consistent simulation of mixed electrical and optical circuits and systems. Drawing on the use of modified nodal analysis (MNA) techniques ubiquitous in circuit simulation, an optical node is formulated which includes the magnitude and phase of the optical signal being simulated. This node consists of two propagating complex envelopes one for the forward direction and the other for the reverse direction. Using this formulation models are developed for a variety of devices including: lasers, photodiodes, multimode fiber, and optical connectors. The formulation allows for definition of multiple optical channels at different carrier frequencies, enables quick simulation of systems with large optical delays and optical interference effects. Several numerical examples are presented in this paper to illustrate the capability of the proposed framework and where practicable the results were compared to commercial simulators. These examples include a multimode fiber optical link, an integrated array of laser sources and a feedback controlled laser source used in a optical link with modulation achieved by the use of an electro-absorption device.**

***Index Terms*—Circuit simulation, electrothermal effects, integrated optoelectronics, laser thermal factors, multi-physics simulation, optical communication, optoelectronic devices, opto-electronic feedback, photothermal effects.**

I. Introduction

THE recent past has seen a rapid growth of complexity and capability in the field of electronics. In particular operating frequencies of devices have continued to increase leading to the presence of high-frequency effects. These signal-degrading effects along with large pin-out densities at packages motivated research in alternate interconnection techniques using optical interconnects and devices within chips and printed circuit boards (PCBs) [1]–[5]. The presence of optical interconnects at the microelectronic level also necessitates the presence of optical drivers, receivers, modulators, and other optical components along with their electrical counterparts at this level of design hierarchy. This co-existence of electrical and optical components in the microelectronic realm is gradually ushering in an era which will require a very high level of integration between electrical and optical components.

Manuscript received November 09, 2009; revised May 05, 2010; accepted June 01, 2010. Date of publication July 29, 2010; date of current version January 07, 2011. This work was recommended for publication by Associate Editor A. Maffucci upon evaluation of the reviewers comments.

P. Gunupudi and T. Smy are with Department of Electronics, Carleton University, Ottawa, K1S 5B6 ON, Canada.

J. Klein and Z. J. Jakubczyk are with Optiwave Systems Inc., Ottawa, K1S 5B6, Canada.

Digital Object Identifier 10.1109/TADVP.2010.2054089

The drive for higher level integration initially manifested as board and package level integration using hybrid technologies such as system on a package (SOP), and a variety of novel substrate technologies [6]–[9]. More recently, integrated photonic solutions based on Silicon substrates have been investigated. Silicon has a number of natural advantages, chief among them the extremely mature fabrication technology, low cost, and very well developed electrical design environment [10]–[12]. Using a mixture of traditional technology, nano-scale fabrication and organic materials, a wide variety of devices have been proposed for the development of integrated opto-electronic circuits [2]–[5]. The continued development of SOP and silicon photonics will likely lead to the rapid integration of photonic elements and electrical devices at the chip, board, and system level in an effort to lower costs and create new opportunities [13], [14].

A significant advantage of optical systems over electrical systems is the ability to carry information signals in separate channels within the same optical waveguide—be it an optical fiber or a ridge waveguide in an integrated optical solution. Each channel is operated at a different optical carrier wavelength. Such a system is referred to as a wavelength division multiplexing (WDM) system [15]. Essentially, the very large bandwidth of an optical interconnect is divided into a number of regions of smaller bandwidth each characterized by a carrier frequency (also known as center frequency). A variety of WDM configurations are used including dense/coarse WDM using single mode fiber [15], typically for long distances, and single channel or coarse WDM with multimode fiber for more local interconnects [16].

The combination of tight optical-electrical integration, thermal coupling and the need to model optical effects such as interference, reflection and multiple carrier frequencies presents a significant design challenge that needs to be addressed. Design of optoelectronic circuits having a high level of integration between both energy domains requires simulation tools capable of accurately and efficiently handling signal flow across optical and electrical components while capturing mutual interactions between these different energy domains. Several attempts [17]–[21] to simulate optical and electrical components together are present in the literature. Chatoyant is an optoelectronic simulation methodology modeled around a hierarchically heterogeneous system-level simulation framework called Ptolemy [22]–[24]. Chatoyant handles nonlinear elements in the system by representing them using piecewise linear models and forms a linear network for the optoelectronic

system which is then simulated in the frequency domain. iSmile and iFrost perform optoelectronic simulation using a mixed-mode methodology by representing some components in the time domain and other components in the frequency domain. The above-mentioned methods do not pay particular attention to the phase of the optical signal. Without accounting for the phase of the optical signal, optical interference, phase phenomena, and chirp can not be simulated. These effects are essential in determining the performance of modern communication systems.

This paper presents the theory and implementation of a new time-domain optoelectronic circuit/system simulator called *OptiSPICE*. In discussing this simulation framework, this paper proposes a definition of an optical node and presents a methodology to model optical signals for ensuring reliable and self-consistent co-simulation of optical and electrical signals in a single engine. The proposed model for optical signals allows a SPICE-like approach to handle optical components in conjunction with electrical elements. This simulator will be useful for mixed optoelectronic systems currently used in telecommunications, information processing, and sensors. In particular, integrated optical circuits/systems with close coupling of electrical/optical and thermal phenomena is seen as a primary application.

Within this framework optical signals are characterized by a carrier wavelength (referred to as optical channels) and sets of optical modes. For example an optical element such as a multimode fiber may have two channels, one at 1300 nm and a second at 1325 nm. Each channel will be represented by a set of mode shapes—these mode shapes may be numerically or analytically determined. For each individual optical mode, two propagating signals are modelled using four state variables. These variables represent magnitude and phase of the complex envelope of electric field of forward and backward propagating light. This choice of state variables proved to be suitable for inclusion of optoelectronic device models in a SPICE based electrical simulation framework [25]. A detailed discussion on the choice of these state variables will be presented in this paper.

A wide variety of optical and electrical elements were modeled using this framework and several examples were simulated. Circuits consting of linear lumped elements, BJTs, MOSFETS, S-Parameter elements (using recursive convolution), and distributed elements were simulated in conjunction with several optical elements such as fibers, lasers, Mach-Zehnders, modulators, and photodiodes. The simulation framework was successful in capturing complex optical effects such as dispersion, scattering, and interference. In addition, support for the thermal dependence of optical and electrical devices was added and examples integrating optical, electrical, and thermal disciplines were successfully simulated.

The following sections will present details on the basic simulation approach, the implementation of the optical signal infrastructure, and descriptions of characteristic devices. Finally, the capabilities of the simulator will be demonstrated using a wide variety of examples, including an optical link consisting of a laser, multimode fiber and detector, an optical circulator, a wavelength division multiplexing circuit, and a control circuit which stabilizes the output power of a laser with respect to temperature variations.

II. Optical Signal Infrastructure

Electrical simulation engines such as SPICE [25] solve electrical circuits by converting equations governing electrical devices into a set of nonlinear algebraic differential equations and representing them in a matrix form through a modified nodal analysis (MNA) type of formulation [26]. MNA equations are typically formed at each electrical node using Kirchhoff's current law (KCL). This type of a formulation is possible because the E and H fields are conservative in the electrical domain. Matrices and nonlinear functions are then determined for a particular device relating port voltages and currents. These relationships are referred to as an element "stamp." Global matrices are formed by "stamping" each element. For an electrical circuit the state variables in the MNA formulation are typically node voltages, currents and device charges.

The global matrices are then simulated in the time domain by using an integration technique such as Backward Euler, Trapezoidal Method or Gear's Method [25]. At each time point, Newton Raphson iterations are used to solve the set of nonlinear difference equations formed by the chosen integration method to arrive at a valid solution. Nonuniform time stepping algorithms are used to simulate the circuit efficiently while preserving accuracy. Alternatively, after a dc solution is found, the system equations can be linearized and a small-signal analysis can be performed.

To incorporate optical signals into this framework, an appropriate choice of representation of the electrical and magnetic field of light must be made. However, it has to be noted that the electrical and magnetic fields in optical devices are nonconservative unlike their electrical counterparts. As such these fields cannot be represented by variables such as voltages and currents. The following subsections explore the issues related to representing optical signals in a SPICE framework and present a viable choice of state variables to represent the electric and magnetic field within an MNA-approach.

A. Modulated EM Waves

An optical circuit is formed of a network of elements, most of which can be described as guided-wave devices. Such devices constrain the optical energy to flow either forwards or backwards along the waveguide. Examples are lasers, ridge waveguides, optical fibers, filters, and modulators. Within such a network, optical signals are propagated from device to device. The solution of Maxwell's equations provides the physical nature of these signals. Solving these equations for a waveguide shows that the optical energy will propagate in modes of the form [27], [28]

$$\mathbb{E}_F(x,y,z,t) = E_F(t)S_i(x,y)e^{i(n'kz+\omega t+\phi_F(t))}$$
$$\mathbb{E}_B(x,y,z,t) = E_B(t)S_i(x,y)e^{i(n'kz-\omega t+\phi_B(t))}$$

where $S_i(x,y)$ is the normalized mode shape determined by the cross-sectional geometry of the waveguide, $E_F(t)$ and $E_B(t)$ are the time varying envelopes of the forward and backward travelling signals respectively, with $\phi_F(t)$ and $\phi_B(t)$ the corresponding time varying phases, ω the carrier frequency, n' the effective optical index of refraction for the mode, and k the wave

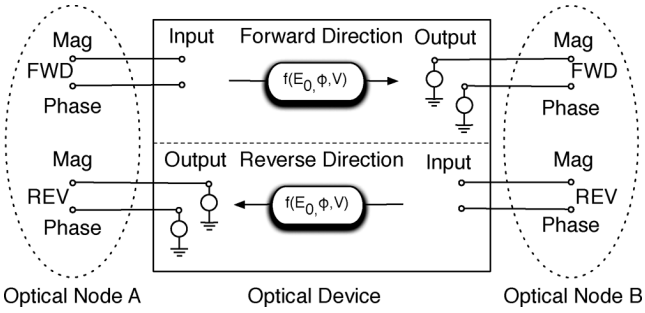

Fig. 1. Single optical link for a signal between two optical nodes.

number. An optical signal therefore consists of an electro-magnetic wave oscillating at a carrier frequency propagating along a waveguide modulated by an envelope of lower frequency. Specifying a position of interest z_0 and integrating over x and y, this signal can be represented as

$$\bar{E}(t,z_0) = E_F(t)e^{i(n'kz_0-\omega t+\phi_F(t))} + E_B(t)e^{i(\hat{n}kz_0+\omega t+\phi_B(t))}$$

where $\bar{E}(t,z_0)$ is the total electric field of light at a particular point in the optical device. The fixed phase shift of $n'kz_0$ for each wave can be absorbed into the $\phi(t)$ terms and the signal can be presented as

$$\bar{E}(t,z_0) = E_F(t)e^{i\phi_F(t)}e^{-i\omega t} + E_B(t)e^{i\phi_B(t)}e^{i\omega t}$$

the sum of two counter propagating waves each with a complex modulated envelope.

This formulation which includes the carrier frequency in the signal (typically in the Terahertz range) gives rise to extremely small time steps during simulation. It is therefore desirable that the carrier frequency be removed when representing the signal and the envelope used. As the forward and backward travelling waves represented by these envelopes are independent (for a linear element), the total optical signal can be modelled as two signals each uni-directional in nature. However, information related to the phase of the envelope needs to be retained as it is instrumental in modeling complex optical effects such as interference and diffraction. In view of the above, it is sufficient to represent the forward signal by $E_F(t)e^{i\phi_f(t)}$ and the reverse signal by $E_B(t)e^{i\phi_b(t)}$.

An optical signal can therefore be characterized by four state variables describing its complex envelope; the magnitude and phase of the forward and reverse travelling signals. These optical nodes must be linked by elements(devices) that maintain the uni-directional nature of these signals.

B. Variables Representing the Complex Envelope

An illustration of a single bidirectional link is shown in Fig. 1. The figure shows a simple link between two optical nodes through a linear optical device in which the output is a function of the input phase and magnitude and other state variables represented by V. In this figure the complex envelope is shown as being represented by the phase ϕ and the magnitude of the electric field E_0. An alternative choice would be to use the real and imaginary parts of the electric field E_r and E_i. The selection of variables representing the complex envelope has important implications on the implementation of the simulator and its effectiveness. Some devices operate on the phase and magnitude of a signal independently and are more naturally implemented (and are often linear) if these variables are used. Other devices, in particular interference based devices, have to be implemented with at least an implicit use of the field values. For example, interference based devices which add optical signals will be linear devices if implemented using the quantities E_r and E_i, but will be nonlinear if phase and magnitude are used. However, the most important consideration is the ability of the simulator to take large time steps and make efficient use of nonuniform time stepping.

Typical optical sources, such as solid-state lasers, have a constant chirp $(d\phi)/(dt)$ at steady-state. This chirp can be quite large (of the order of 10^{12} radians/s) which results in, even at steady-state, a sinusoidal variation of optical fields E_r and E_i at these frequencies. Therefore, the use of these fields as state variables will limit transient step sizes to well under a nanosecond even when the circuit is essentially quiescent. Optical circuits often involve a wide variety of time constants with both extremely short pulses and long delays. This renders simulation of fibers and waveguides inefficient when the real and imaginary parts of the envelope are used as state variables.

The alternative of representing the complex envelope using its magnitude and phase enables the use of large time-steps during simulation. At steady-state, the phase variation is The use of magnitude and phase as state variables thus overcomes the issue of small step sizes during simulation. However, a consequence of this choice is that optical elements involving the interference of signals (where the fields of two signals need to be added in the complex domain) are nonlinear due to the need to involve sines and cosines of the phase. It was found that the computational time saved by enabling larger step sizes far outweighs the computational time spent by the simulator in treating interference and mixing devices as nonlinear elements.

C. Phase Variable

The use of phase as a state variable does, however, present a number of issues that have to be addressed. Phase is a band limited variable and for the simulator to be efficient it must be a continuous and smooth function. For sources such as lasers, this is generally not an issue as the phase is determined by a differential equation that naturally produces a continuous smooth function. However, with other devices that determine the phase from field components, such as an optical joiner/splitter, care must be taken to ensure that no discontinuities at $-\pi$ and π are present. For instance, when evaluating the phase from real and imaginary parts of the electric field, an equation such as $\phi = \Delta\phi + n_w \cdot 2\pi$ must be used where $\Delta\phi$ represents the band limited phase determined from the $\arctan$ of E_i/E_r and where n_w determines the particular 2π band that the phase value is to be placed in.

D. Channels, Modes, and Mode-Shapes

Having defined an appropriate optical signal representation, a number of complications need to be addressed. For most optical devices (such as a waveguide) the optical energy will propagate on an infinite set of orthogonal electromagnetic modes with the

cross-sectional mode shape defined by the device geometry and possibly the wavelength of the optical excitation (the carrier wavelength) [28]. Each mode is an independent signal which will propagate through the device. Although the set of modes is infinite, only a finite subset will be excited with a significant amount of energy.

At this point it is useful to define a mode-structure which represents the signal propagation through a device at a particular carrier frequency. A mode-structure is therefore a set of optical signals, each consisting of the magnitude and phase of the complex envelope (for both forward and reverse traveling waves) and the mode shape associated with each signal. The mode-structure depends on the geometry of the optical component and the nature of the optical excitation. For simple geometries analytical mode shapes such as Bessel functions can be appropriate. For more complicated situations numerical mode solvers based on 2-D solutions of Maxwell's Equations can be used. Existing mode solvers available in the market can be coupled relatively easily with this framework and determining the modes of optical components is usually straight-forward. A final complication in the mode structure is polarization. In the *OptiSPICE* format each mode structure can support either one polarization (X) or two (X and Y). When two polarizations are specified the signal structure is doubled producing twice the number of independent signals.

Due to the desire to model systems with WDM configurations a channel infrastructure needs to be specified. The number of channels present in a particular device will be determined by the circuit topography. Within *OptiSPICE* an optical device will therefore contain a number of channels. Each channel defines a mode-structure and a state variable whose value is equal to the particular carrier frequency of the channel.

As described previously each individual optical signal is composed of four state variables identified with forward and backward propagating complex signals described by magnitude and phase for each polarization. Therefore, a mode-structure which contains n_m modes will have $8 \times n_m + 1$ state variables (the optical signals for both polarizations plus the carrier frequency variable). A particular optical device with n_c channels will have $n_c \times (8 \times n_m + 1)$ state variables associated with the optical propagation.

These state variables can be used to calculate the total electric field at an optical node at any time-point of interest if so desired. In order to calculate the electric field, the complex envelopes represented by magnitude and phase, for each mode in every channel, are modulated at the carrier frequency and multiplied with their corresponding mode-shapes. These waveforms are summed to obtain the total electric field present at the optical node.

III. Device Models

Models for electrical devices are well developed for SPICE-based electrical simulation frameworks [25]; these models have been incorporated into the *OptiSPICE* framework that match industry standards for electrical compact models. These models include bipolar and field effect transistors, passive components, sources and transmission lines. Optical models on the other hand have to be developed for this new infrastructure.

For convenience, this paper classifies optical models into three broad categories based on how they manipulate input signals to produce output signals. The simplest type of optical models take the magnitude and phase of optical inputs and perform operations such as attenuation, delay and dispersion on them—an example of such a device is a multimode fiber. Models for these devices are termed *direct*; these devices do not model interference effects and do not perform conversion of the signal from one energy domain to the other. Sources and detectors are the second class of devices and connect signals from one energy domain to another. These elements can either be simple linear elements or, as for a diode laser, complex and nonlinear. The third category of devices linearly mix (add) optical signals, this is the case with optical connectors and cross-couplers and interference based devices. Models for these devices must take the input magnitudes and phases and internally convert them into real and imaginary parts (without introducing their corresponding state variables) and then use nonlinear operations such as sines and cosines in order to evaluate the fields leaving the output node.

This subsection briefly presents the development of optical models for some commonly used optical devices and elements.

A. Direct Elements

As mentioned above, these optical models take the magnitude and phase at the input of the optical device and perform several operations such as delay, attenuation, and dispersion on these quantities in order to evaluate the magnitude and phase at the output of the optical device.

In order to illustrate the modeling of a direct element, a multimode fiber is taken as an example. This model uses delay elements, attenuation and phase-shifters to model the behavior of a multimode fiber and follows the work in [29]. Details of this model are shown in Fig. 2. The first figure shows the signal organization for the fiber with two channels. Within each channel there are n_m optical modes present and each mode is bidirectional. Where n_m is chosen to be large enough to accurately model the optical field. The second figure shows a detailed model of one of the modes in a channel. This figure illustrates how the two state variables are connected. The magnitude of each mode is isolated, attenuated and delayed. The delayed magnitude represents an envelope delay that could vary from nanoseconds to seconds depending on the length of the element. The implementation of this delay makes uses of the stored history of the element and the known delay for each mode in the fiber. The second state variable (phase) is passed through the element with the addition of a phase shift which represents the shift of the phase from the input to the output. The magnitude of these delays is determined from the length of the fiber and the effective index of each mode. In this model, the total delay of the signal is therefore split into two parts, an envelope delay and a phase delay. Envelope and phase delays are uniquely specified for every mode in the fiber. The envelope delay is calculated by determining the total phase delay present for a mode and then associating an integral number of 2π phase delays with this delay. The remainder of the phase delay (which must be between 0 and 2π) is used as the phase shift for the mode. As can be seen in the figure the forward and reverse

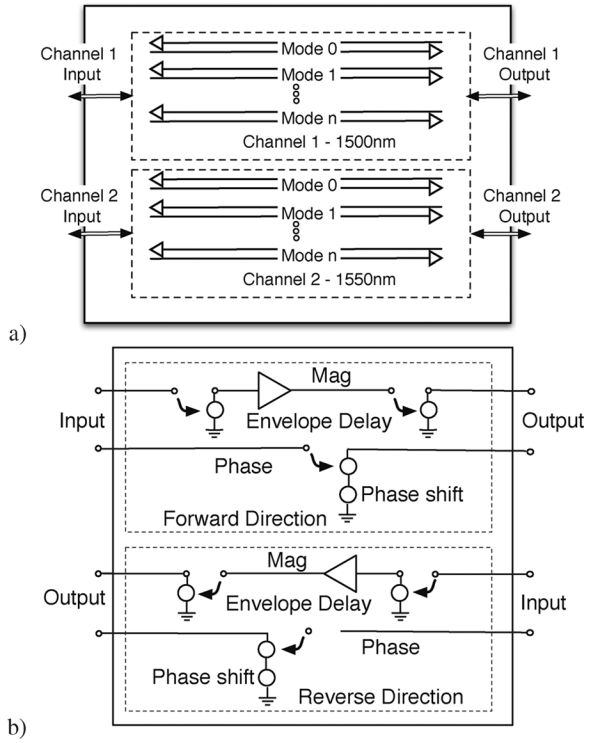

Fig. 2. Model schematic showing (a) A multimode fiber model consisting of two channels each comprised of n modes. (b) The detailed model of one of the modes in the multimode fiber illustrating both the forward and reverse signals.

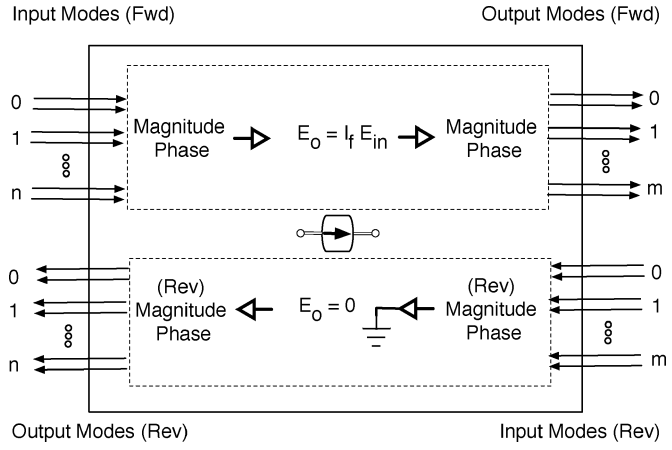

Fig. 3. Model schematic for a single channel optical isolater.

optical signals are explicitly uni-directional with isolation provided by "voltage controlled voltage sources" at the inputs.

A second example of a linear element is presented in Fig. 3. This element is a uni-directional opto-isolator which passes the optical signal in one direction only. It essentially "grounds" the signal in one direction (for this element the reverse direction was chosen). This element is a particular instance of a more general element that allows for independent gain or attenuation of a signal in either direction. Although an idealized device, the optical isolator is useful in building optical circuits.

The two examples given above for *direct* elements are linear, of which another example would be a simple mirror that reflects a signal with or without a phase shift. However, independent elements can also be nonlinear. With such a device, the relationship between the input and output phases and magnitudes can be complex, nonlinear, and dependent on other inputs such as voltages and currents. The stamps for these elements involve nonlinear functions. Models for these elements need to be created in a way so as to be compatible with the *OptiSPICE* framework, physically accurate and preferably not computationally intensive.

An example of such a case is an electro-absorption modulator (EAM) which is typically used to modulate a constant amplitude optical source to produce a bit stream. An EAM functions by applying a bias voltage to semiconductor ridge waveguide structure altering the concentration of photo-generated carriers (N) present in the structure. The complex index of refraction $(\bar{n} = n_r + in_i)$ of the waveguide is a function of number of carriers present and the applied electric field. Changing the applied bias thus produces a variation in both phase and amplitude of the propagating signal and can be used to suppress or modulate the input optical signal. The degree of modulation of the optical signal is directly related to the length of the waveguide. For an incident signal $E_i e^{i\phi_i}$ on a device characterized by a length L and wavevector k_0, where n_r and n_i are both functions of the applied bias V_A and N, we have for the propagation of a single optical signal through the waveguide, the following expression for the output field [30]:

$$E_o e^{i\phi_o} = E_i e^{-k_0 L n_i} e^{i(\phi_i - k_0 L n_r)} \tag{1}$$

where $\Gamma = 2k_0 L n_i$ is a loss coefficient and output phase is $\phi_o = \phi_i - k_0 L n_r$. For an EAM n_i and n_r are complicated functions of N and V. Typically, a device is characterized by measuring the attenuation and chirp as function of V and the incident optical power $S_i = E_i^2$. Using such measurements two parameters $\Gamma(V, N)$ (which defines the loss) and $\alpha(V, N)$ (a chirp coefficient) can be determined.

Using these parameters a physical model of the EAM [30] can be specified. An internal rate equation determines the number of photo-carriers

$$\frac{dN}{dt} = \frac{\lambda}{hc} e^{-\Gamma_c} \left(1 - e^{-\Gamma(V,N) + 2\Gamma_c}\right) S_i - \frac{N}{\tau} \tag{2}$$

where λ is the optical wavelength, c the speed of light, h Planck's constant, Γ_c the fiber facet loss, and τ the carrier lifetime. The magnitude and phase of the output field are determined by

$$E_o(t) = E_i e^{-\Gamma/2} \tag{3}$$

$$\frac{d\phi_o}{dt} = \frac{\alpha(V,N)}{2} \frac{d\Gamma(V,N)}{dt}. \tag{4}$$

The stamp of the EAM is created by declaring a state variable to represent N and using (2) to place the appropriate terms in the $\mathbf{C}$ and $\mathbf{G}$ matrices along with a nonlinear source in the vector $\mathbf{B}$. The value of the output field is easily determined from (3). The chirp is then obtained using (4) and added to the initial phase to determine the final phase of the field. Although this description is for the forward propagating signal in a single mode device, a similar set of equations describe the operation of a multimode bidirectional structure and can be obtained by a straightforward

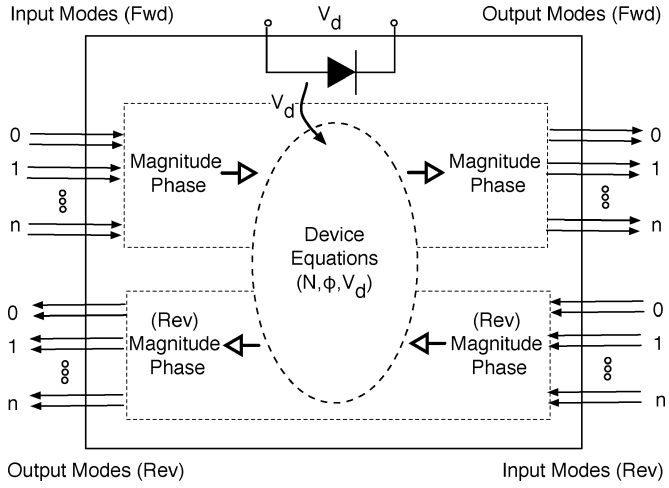

Fig. 4. Model schematic for a single channel Electro Optical Absorber.

extension. The electrical submodel used for the EAM is a diode or open circuit with an optional input circuit consisting of a resistor, inductor and capacitor. A schematic model of the device is presented in Fig. 4.

B. Optical Sources and Detectors

Two types of sources were implemented using the *OptiSPICE* infrastructure. The first is a diode laser (DL) and the second is a simple fictitious source referred to as constant wave (CW) source defined for convenience. The CW source can be used to feed waveforms into optical components without the need for a diode laser and its driver circuit.

Diode Laser: The diode laser source is modeled in detail in the *OptiSPICE* framework using its physical, electrical and optical device equations. A physically based model of a (single mode for simplicity) laser diode can be defined using rate equations for the electron and photon densities and optical phase [31], [32]

$$\frac{dN}{dt} = \frac{\eta(I_d - I_{\text{off}})}{qV_l} - \frac{N}{\tau_n} - \frac{G_0(N-N_0)P_i}{1+\epsilon P} \tag{5}$$

$$\frac{dP}{dt} = \frac{\Gamma G_0(N-N_0)P}{1+\epsilon P} - \frac{P}{\tau_p} + \frac{\Gamma\beta N}{\tau_n} \tag{6}$$

$$\frac{d\Phi}{dt} = \frac{1}{2}\alpha\left(\Gamma G_0(N-N0) - \frac{1}{\tau_p}\right) \tag{7}$$

where η is the injection efficiency, I_d the diode current, V_l the laser volume, N the number of carriers, τ_n and τ_p are the electron and hole lifetimes, G_0 the gain coefficient, P the photon density, Γ the mode confinement factor, β the spontaneous emission coefficient, α the linewidth enhancement factor, and ϵ the gain compression coefficient. Following [32], a temperature dependent offset current defined by a polynomial

$$I_{\text{off}} = a_0 + a_1 T_l + a_2 T_l^2 + a_3 T_l^3 + \cdots \tag{8}$$

accounts for static thermal effects with the coefficients $a_0 \ldots a_n$ determined from parameter extraction.

A schematic showing the internal details of the laser model is presented in Fig. 5. The laser thus consists of a diode, three rate

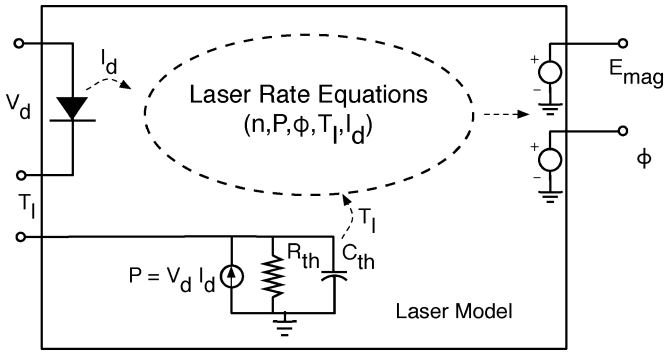

Fig. 5. Model schematic for a single mode laser.

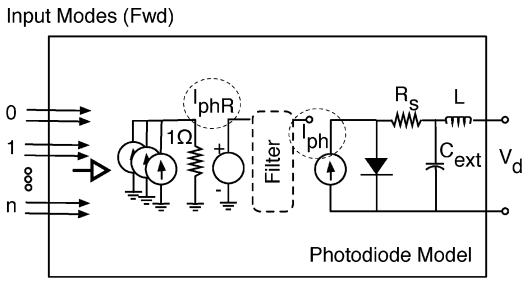

Fig. 6. Model schematic for a single channel multimode photodiode.

equations, and a thermal subcircuit. This laser model is temperature dependent and models a wide variety of effects. The resulting model has internal state variables for photon density, carrier density, and device temperature. The output is an optical field magnitude and phase. Using these variables, the rate equations governing the laser diode's behaviour are stamped into the MNA matrices.

CW Source: The CW source has a defining carrier frequency and two electrical ports that determine the magnitude and phase of the optical output. The source can be operated in a number of modes. The simplest implementation linearly relates each input voltage to the two optical output variables of phase and magnitude—in this mode the device is linear. When using the second mode the two voltage inputs control the phase and the output optical power and the device is nonlinear with respect to the magnitude but linear for the phase variable. For the third mode the electrical inputs are linearly related to the output field components E_r and E_i and in this case both optical outputs are nonlinearly related to the inputs. The CW source can be used in either single mode or multimode operation and can be specified to be produce singly or doubly polarized optical signals.

Photodiodes: Detectors are modeled using an electrical diode and a photo-current which is proportional to the optical intensity at the input. The relationship of the photo-current to the optical intensity is given by a frequency domain filter response [33] that is synthesized into a circuit. In the implementation (shown in Fig. 6) a set of nonlinear current sources each having a magnitude determined by the square of the electric field magnitude associated with an optical input mode are summed by connecting them to a 1-Ω resistor. The resultant voltage across this resistor has the value i_{phR} and is then passed through the filter to obtain a voltage equal to the photo-current. This voltage then drives

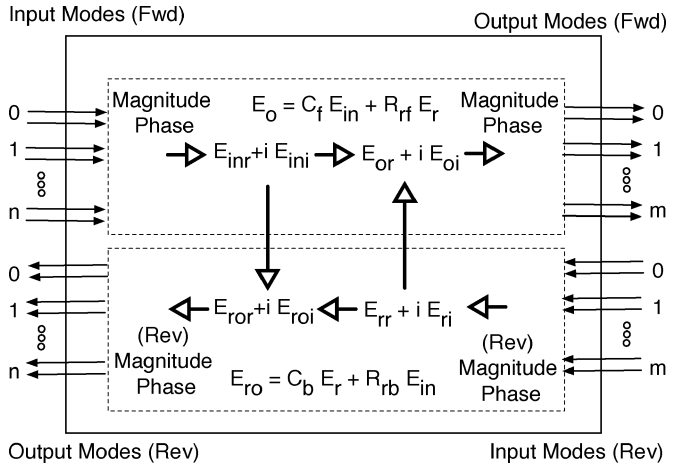

Fig. 7. Optical Connector Model for a single optical channel matching n input modes to m output modes.

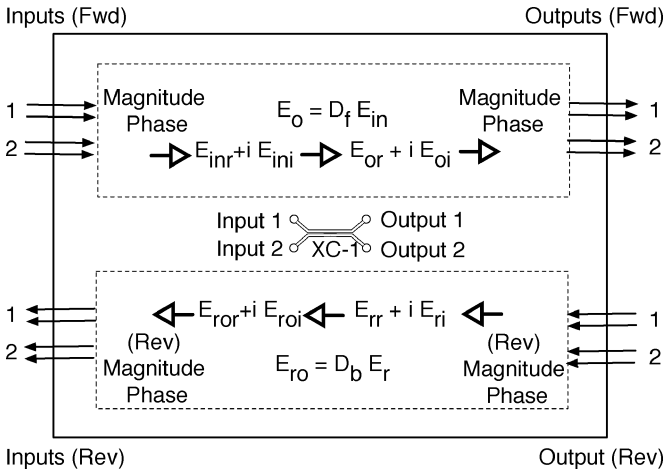

Fig. 8. Single channel optical cross-coupler model.

a nonlinear source in parallel with a SPICE diode. This configuration with addition of series resistance, inductance and an external capacitance forms the photo-diode model.

C. Interference Based Elements

An important class of elements are ones that "mix" or add optical signals together. Modeling of mixing elements is illustrated in this subsection using an optical connector and a optical cross-coupler.

Optical Connector: A typical optical connector is shown in Fig. 7 and models the connection of two optical devices such as a laser and a fiber. At such optical interfaces where components interact, the mismatch between mode structures will produce reflections, scattering, and transmission. The optical connector element is used to take the modal information from the input device described by a set of mode shapes $\hat{I}_i(x,y)$ and map this information to the modes of the output device represented by the mode shapes $\hat{O}_j(x,y)$. This mapping is done through a set of complex coefficients $(\bar{C}_{ij})$ which form a connection matrix $\bar{\mathbf{C}}$.

Therefore, for all optical connectors, the values of the $\bar{\mathbf{C}}$ connection matrix must be calculated. This matrix relates the input and output complex envelopes for each mode such that $\bar{O}_j = \bar{C}_{ij}\bar{I}_i$. The coefficients of this matrix represent the percentage of the energy from the jth input mode that excites the ith output mode. The coefficient can be calculated using an overlap integral of the form [28], [34]

$$\bar{C}_{ij} = \int\int \hat{O}_i(x,y)\hat{I}_j(x,y)dxdy. \tag{9}$$

If the input and output mode structures are the same, then due to the orthonormal nature of the modes the $\bar{\mathbf{C}}$ matrix will be an identity matrix and no mixing will occur. As some of the optical energy may be reflected, absorbed, or scattered, the total output energy may be less then that of the input.

Fig. 7 illustrates how the output signals for forward and reverse directions are determined within a single channel in this device. As shown, the forward travelling input mode signals (represented by phase and magnitude) are converted to real and imaginary fields E_{Ir} and E_{Ii} as are the reverse travelling incident signals E_{Rr} and E_{Ri}. These fields are then multiplied by the complex matrices $\bar{C}_f$ and $\bar{R}_r$, respectively, and added to obtain the output fields E_{or} and E_{oi}. These fields are then converted to output phase and magnitudes. The matrix $\bar{C}_f$ represents the mode coupling between the input and output and is calculated using overlap integrals during the preprocessing of the circuit. The matrix $\bar{R}_r$ represents the reflection (including a possible phase shift) of the incoming modes. It is important to note that the element is nonlinear due to the conversion of phase and magnitude to field components and that no internal state variables representing these components are used.

For most situations, calculations of the matrices $\bar{\mathbf{C}}$ and $\bar{\mathbf{R}}$ are independent of the actual system simulation. They can then be calculated in the preprocessing stage prior to simulation. Indeed, these calculations can be quite computationally intensive. Very often, however, during the design process multiple simulations will be done with identical devices and configurations. Under this situation it is useful when generating $\bar{\mathbf{C}}$ and $\bar{\mathbf{R}}$ to note the conditions under which they were calculated and then cache them on disk using a unique identifier. In a subsequent simulation they can then be read and used directly with no need to generate them.

Optical Cross-Coupler: The second common situation in which optical "mixing" occurs is in devices with multiple inputs and outputs such as joiner/splitters and cross-couplers. An optical cross-coupler is a device that physically couples two input signals and produces two output signals. For the sake of simplicity, the model of a single-channel, single-mode element is presented as an example in Fig. 8. A basic cross coupler element has two inputs and two outputs, no mode coupling and the output fields are related to the input fields by [35]

$$\begin{pmatrix} \bar{E}_{o1} \\ \bar{E}_{o2} \end{pmatrix} = \begin{pmatrix} \sqrt{1-c} & p\sqrt{c}\cdot i \\ p\sqrt{c}\cdot i & \sqrt{1-c} \end{pmatrix} \begin{pmatrix} \bar{E}_{i1} \\ \bar{E}_{i2} \end{pmatrix} \tag{10}$$

where p and c characterize the cross-coupler. Therefore, for this device, the inputs are mixed into each output and conversely for the reverse direction, the outputs are mixed onto the inputs.

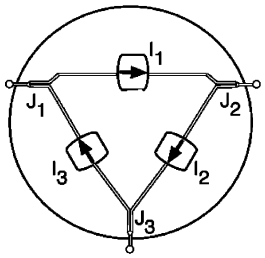

Fig. 9. Optical circulator formed as a complex element.

This mixing is represented by the matrices $\mathbf{D_f}$ and $\mathbf{D_b}$ which perform the mixing for all modes in the channel and are created by applying the relationship presented in (10).

An optical splitter/joiner can also be implemented in such a structure. For example for a 3 db splitter/joiner that conserves power, having one input and two outputs, the relationship between the forward travelling waves for the two output fields and the input would be

$$\begin{pmatrix} \bar{E}_{o1_F} \\ \bar{E}_{o2_F} \end{pmatrix} = \frac{\sqrt{2}}{2} \begin{pmatrix} 1 \\ 1 \end{pmatrix} (\bar{E}_{i_F}) \tag{11}$$

and in the backwards direction

$$(\bar{E}_{i_B}) = \frac{\sqrt{2}}{2} (1 \quad 1) \begin{pmatrix} \bar{E}_{o1_B} \\ \bar{E}_{o2_B} \end{pmatrix}. \tag{12}$$

The examples of mixing elements illustrated above are specific instances of a generalized signal-mixing element implemented in *OptiSPICE*. This element allows the linear mixing of optical fields from N inputs with M modes to K outputs with L modes. This generalized element allows for a very general linear mixing of multiple inputs and outputs modes and signal reflections. It can also be used to define linear gain/attenuation elements, to characterize optical loss and model diffraction through free space regions. When this device is implemented, it has to be treated as a nonlinear element due to the presence of trigonometric functions. However, derivatives of these trigonometric functions are well-behaved and work well within the Newton–Raphson nonlinear solver used in the engine. One complication, as mentioned before, is that the output phases determined by are band limited to $-\pi$ to π and care must be taken to make the output phase continuous by keeping track of the number of 2π traversals that have undergone during the transient simulation.

D. Complex Elements

It is also possible to form complex elements from the basic elements described above in a manner analogous to electrical sub-circuits used in SPICE. Fig. 9 presents a model of an optical circulator formed of three optical isolators and three joiner/splitters. This three port device can be defined to be an ideal device with no loss present in the joiner/splitters and isolators or with nonidealities. Reflections, either external at the interface ports, or internal at the isolators can also be defined.

IV. Formulation of System Equations

The simulation of an optoelectronic network using this methodology is divided into two stages. These stages are explained in the following subsections.

A. Preprocessing Engine

The first stage involves preprocessing the optical network. This stage is used to form a network of optical channels, each representing a specific carrier wavelength. Starting from optical sources, channels are traced through the network and each device is updated with information on what channels it contains. Once the channel architecture is created, optical mode-shapes can be determined. These mode shapes must then be used to calculate scattering and reflection values present at optical interfaces between devices. Optical mode overlap integrals are used to determine the coefficients of optical reflection and transmission matrices for these interfaces. At this point, a number of other elements, such as free space diffraction elements, will also need to be processed in order to be characterized. After this stage is completed each component will be fully described and system equations can be created.

B. System Equations

The system equations are formed in a manner identical to MNA formulation used in electrical circuits. Each element is described by a stamp which has linear and nonlinear components. Each element is processed and stamped into the global system equations that have the from

$$\mathbf{C}\frac{d\mathbf{x}}{dt} + \mathbf{G}\mathbf{x} + \mathbf{F}(x) = \mathbf{B}(\mathbf{t}) \tag{13}$$

where $\mathbf{C}$ represents the energy storage elements in the system, $\mathbf{G}$ is the conductance matrix, $\mathbf{B}$ is a time dependent forcing function, $\mathbf{F}(x)$ captures the nonlinear nature of the devices, and x is the vector of unknowns.

Of particular importance is the presence of delay elements in optical devices. Using the complex envelope formulation, this delay can be represented either as an envelope delay (a delay in the magnitude of the field) or as a phase shift. Depending on the magnitude of the delay, either approach or a combination of both may be appropriate. The implementation of envelope delay requires the retention of a device's "history." This history can then be used to determine the output of the device. A phase delay is simply implemented as a phase shift between the input and the output of the device.

The infrastructure described above was found to be capable of accommodating the modeling of a wide variety of optical devices. These include optical fibers (single and multimode), interference devices such as Mach-Zehnder interferometers, sources and detectors and a variety of circuit configurations including wavelength division multiplexing (WDM). Postsimulation, optical signals can be processed to provide information on optical power, signal bandwidth, optical phase, and chirp.

Once the opto-electronic system equations are formed (13) can be simulated using traditional simulation techniques.

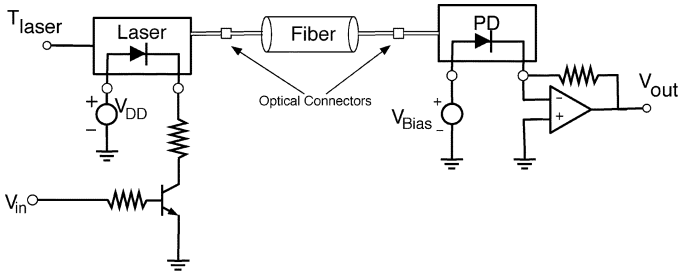

Fig. 10. Optical multimode fiber link schematic with laser driver and detector.

V. Numerical Results

To confirm the accuracy of models used in *OptiSPICE*, individual devices were simulated under very simple conditions and compared to published results. A large number of purely electrical circuits varying from amplifiers and oscillators to transmission lines have been verified with a commercial version of *SPICE* [36]. The laser model was compared to data provided in Cartlidge *et al.* [31] and Mena *et al.* [32] and was found to be accurate and robust. Results in Cheng *et al.* [37] were used to confirm the accuracy of the electro-absorber model. The optical connector and multimode fiber models were verified by the use of OptiSystem [38] a commercial optical system simulator.

In the remainder of this section a number of examples are presented to illustrate the capabilities of the opto-electronic simulation framework presented in this paper. For the simpler circuits these results will be compared to simulations obtained by the use of HSpice [36] and OptiSystem [38] to confirm the accuracy of the simulations.

A. Simple Optical Link

The first example (shown in Fig. 10) is a simple optical link consisting of a bipolar junction transistor (BJT) driving a laser diode with a Gaussian optical mode. The laser is connected to a multimode fiber where simple Bessel modes are assumed. The output of the fiber is connected to a photodiode that converts the optical signal into an electrical current which is subsequently converted to a voltage using a trans-impedence amplifier. The fiber/laser and fiber/photodiode connections are represented using optical connectors which model reflection and transmission of the optical power. This example requires a self-consistent solution of the electrical circuit and the optical link. To illustrate the use of the simulator to model short optical pulses travelling through a multimode fiber, Fig. 11 presents the input current pulse driving the laser and the output current signal from the photodiode. The initial pulse is 0.8 ps in length with rise and fall times of 0.2 ps. The fiber delay is nominally 3.0 μs, with moderate mode dispersion. As can be seen from the figure, the pulses are resolved with time-steps around 1.0 fs while time-steps as large as 0.1 μs are taken to simulate the part of the response that is essentially quiescent. Also shown in the inset for the input pulse is a *Spice* [36] response for the laser driver circuit. The time stepping of the *Spice* simulation was significantly coarser due to the lack of the complex laser response present in the *OptiSPICE* simulation. However, the two simulators predict the same response for the circuit.

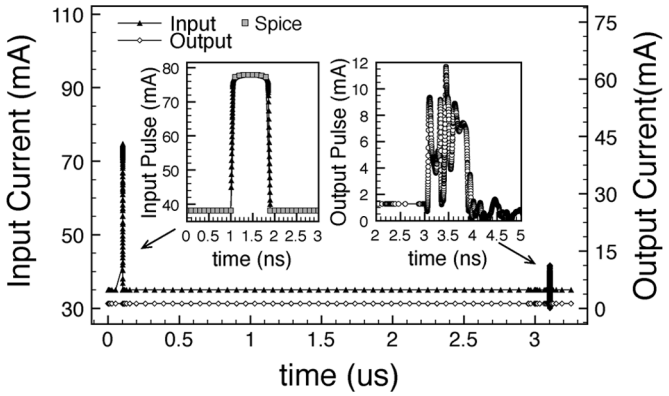

Fig. 11. Input and output current pulses for optical link example. For inset figure the time axis is shifted. For the inset input pulse, both *OptiSPICE* and *SPICE* simulations are shown.

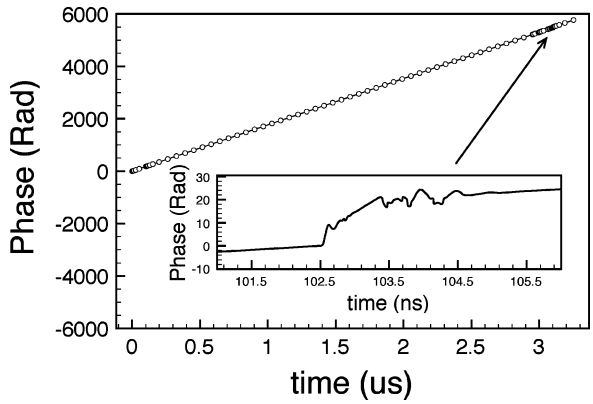

Fig. 12. Optical Link: Phase at the fiber output. Inset figure has a shifted time axis.

As discussed in Section II-B, the phase and magnitude of the complex envelope of the optical signal were chosen as the state variables. The phase for the first mode at the fiber output is shown in Fig. 12. The linear increase in phase initially is due to the constant chirp of the laser source. This constant and large chirp would prohibit taking large time steps if optical signals were represented using real and imaginary parts of the envelope of the electric field. The inset figure shows rapid variation in the phase of the optical signal due to the laser dynamics as the pulse exits from the end of the fiber.

The magnitude of electric field for the first three modes is shown in Fig. 13(a) and (b) for the input and output of the fiber respectively. In the former figure, the modes are all temporally aligned and linearly scaled with respect to the laser output. The relative magnitudes of these signals are determined from the overlap integrals calculated for the Gaussian laser mode and the Bessel modes of the fiber. The latter figure presents the magnitude of three modes at the output of fiber. The signals are no longer aligned due to modal dispersion.

The inset figure of Fig. 13(b) presents the total optical power (the sum of the modes) present at the fiber output. Also plotted is a result obtained using *OptiSystem* [38]. To obtain this data the input current pulse obtained from the spice simulation was used to drive a rate equation laser model. The output from this

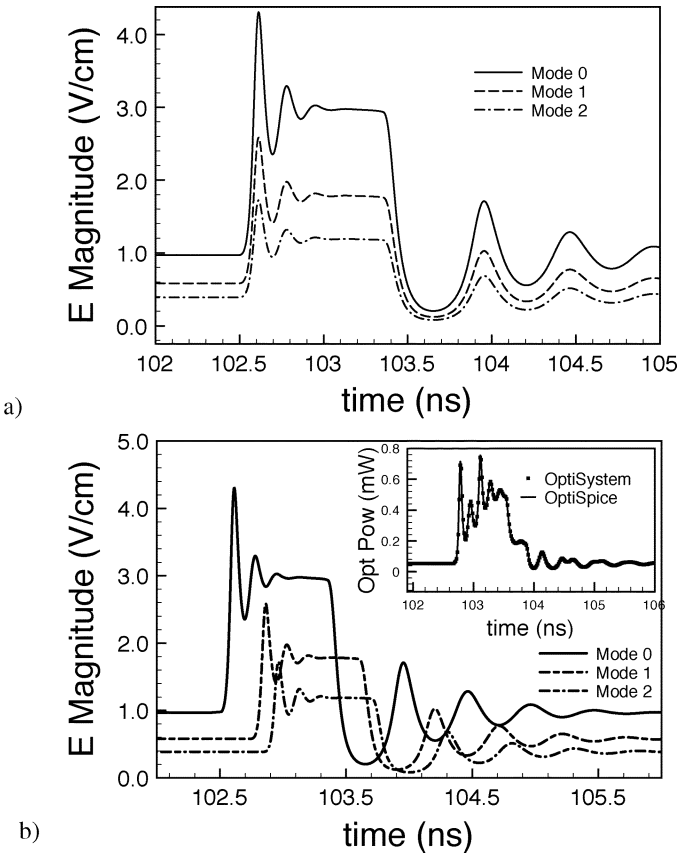

Fig. 13. Optical link: Electric field magnitude for the first three modes (a) At the fiber input. (b) The fiber output (shifted time axis). Inset figure presents the total optical power at the fiber output for both *OptiSPICE* and *OptiSystem* simulations.

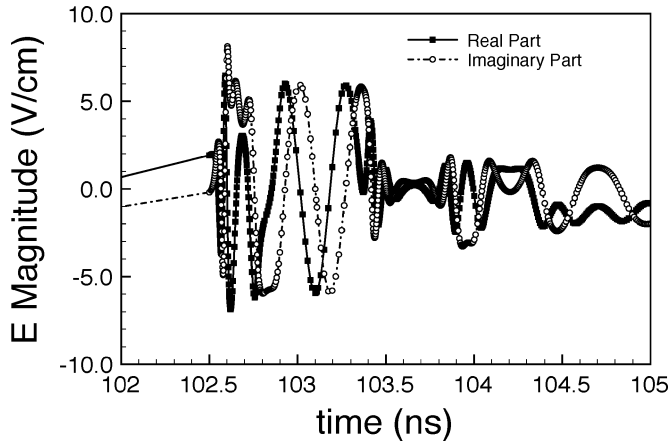

Fig. 14. Optical link: Electric field components for the laser output during the initial pulse.

model was then used as an input into *OptiSystem* and the optical output power at the end of the fiber was obtained.

In Fig. 14, the complex electric field for the fiber input is shown for the initial input pulse. This figure is derived from the state variables of phase and magnitude for the laser optical output. As can be seen from the figure, the electric field response is extremely complex and rapidly varying. It is, however, well captured by the time stepping algorithm.

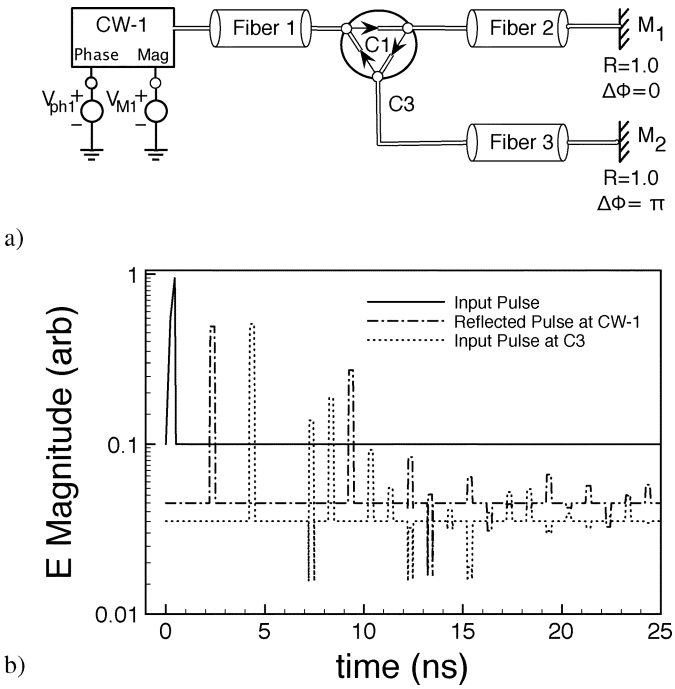

Fig. 15. Circulator circuit example. (a) Schematic. (b) Electric field magnitudes at input and the optical node C3.

B. Circulator—With Reflections

The second example [see Fig. 15(a)] is an optical circuit with a single CW source, three waveguides and an optical circulator. The three waveguides have envelope delays of 1 ns, 1.5 ns, and 2.0 ns, respectively. The mirror used at the outputs of second and third fibers have a reflectivity of one, with the first having no phase shift during reflection and the second a phase shift of π. Each input of the circulator was also assumed to have 25% power reflection with a phase shift of π in the reflected component. The entire system was assumed to be single mode.

Fig. 15(b) shows the result of simulating the optical circuit for 30 ns. The three responses shown in this figure are the optical input at the CW source, the reverse traveling signal at the source and the input at the third port (C3) of the circulator. The output waveforms form a complex response due to the phase shifts and reflections at mirrors and circulator ports. This example demonstrates the ability of this framework to simulate complex reflections and their interference. Comparison of this optical circuit with *OptiSystem* was completed. The results confirmed the accuracy of *OptiSPICE* with the results being found to be almost indistinguishable from the *OptiSystem* simulation.

C. Multichannel WDM Circuit

The example presented in Fig. 16 shows a simple coarse WDM example. This example has eight laser sources—each driven by a BJT circuit and at carrier frequencies equally spaced from 1275 to 1450 nm, an eight input optical mux, followed by a multimode fiber and then a demux connected to eight detector circuits. Each output of the demux has an optical filter that selects a particular optical channel. The lasers and drivers are mounted on a single substrate and thermally coupled through the substrate resulting in differential heating. The simulation

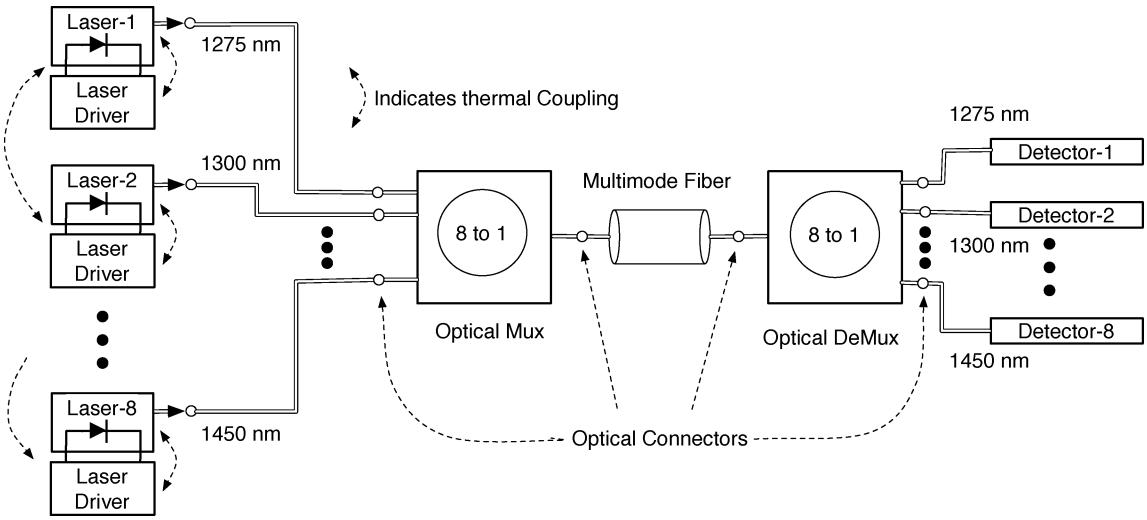

Fig. 16. Multichannel coarse WDM optical circuit system schematic.

involves three distinct energy domains: electrical, thermal, and optical.

As this example has multiple sources operating at different carrier frequencies, during the first stage, the simulator would create the channel topography for the circuit. Starting with source "Laser-1," the preprocessing engine constructs a channel by tracing an optical pathway. As there is a mode mismatch between the laser and waveguide inputs of the mux element, an optical connector is needed to represent mode coupling and reflections present at the interface. The first channel is propagated through this optical connector and the Mux element. The next physical element it encounters is a multimode fiber. Once again as there is a mode mismatch at the interface, an optical connector is needed. At this point, there are two paths to be followed one to the output of the fiber and (if there are reflections) also back to all the input ports of the mux element. Following the first path, the channel will propagate through another optical connector and then to all the outputs of the demux. Following the algorithm through output port 1, the channel is passed to the detector. The detector includes an optical filter which terminates all channels except one which is passed to the photodiode which terminates the remaining channel. The photodiode is placed in an electrical circuit which provides biasing and amplifies the photocurrent. As this path is now complete, the simulator completes the tracing of channel 1 propagating a channel from input ports of the mux back to the other sources which terminate the channel. Following this procedure, the channel topography is traced for all eight channels. Once the channel topography has been determined devices can be fully characterized: mode structures can be determined for all elements and the optical coupling matrices $(\bar{\boldsymbol{C}})$ can be calculated.

This example demonstrates the capability of the simulator to handle multiple channels and also model thermal effects such as self-heating and coupling. Each laser diode in the circuit is thermally coupled to its driver and to its adjacent channels. The lasers are assumed to be fabricated on a single substrate and

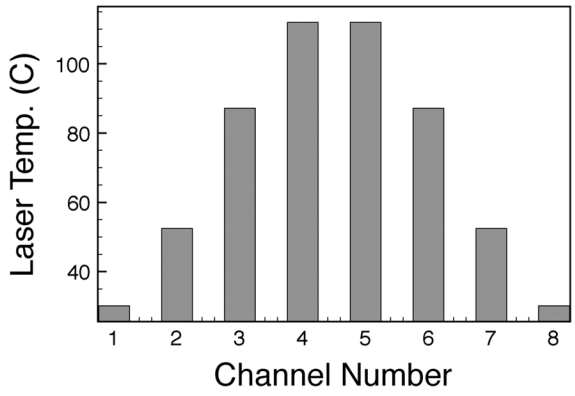

Fig. 17. Laser temperatures for the sources of the coarse WDM circuit.

arranged in a sequential order. Thus the lasers in the center will be at a higher temperature than the ones on the edge.

The temperature of the laser is primarily determined by the average power present in the laser. Fig. 17 shows the steady state temperatures of the eight laser diodes. A variation of 75 K is seen from the edge to the center of the laser array. This variation of temperature has a significant effect on the operation of the individual lasers and optical channels. In Fig. 18, the input current for the laser is shown for laser 1 and 4. The higher temperature of the central laser produces a larger input current for the same stimulus. This results in a variation in the optical output of the laser and for the signals propagated through the circuit. The three remaining plots in Fig. 19 show the optical power, phase and chirp for channels 1 and 4 at the output of the demux. The effect of the temperature variation can be easily seen in these results. Also shown in these plots are results obtained using *Spice* and *OptiSystem*. In the first plot, the laser and transistor temperatures obtained from the*OptiSPICE* simulation were taken for Channel-1 and used to simulate the laser driver circuit in *Spice* by modeling the diode laser with an equivalent diode. As can be seen from Fig. 18(a), the diode currents match accurately. This diode current was then used to drive a rate equation laser

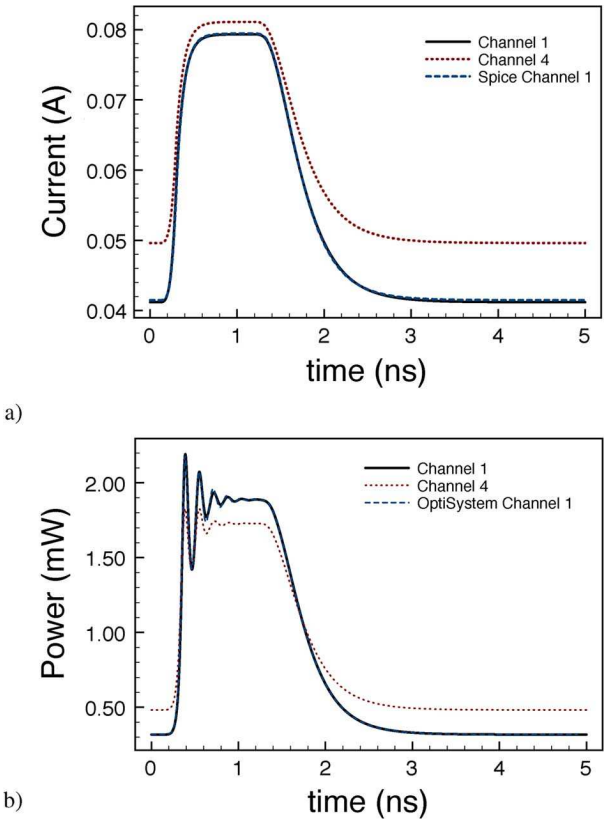

Fig. 18. Coarse WDM example. Transient plots for channels 1 and 4: (a) Input laser currents. (b) Output laser optical powers.

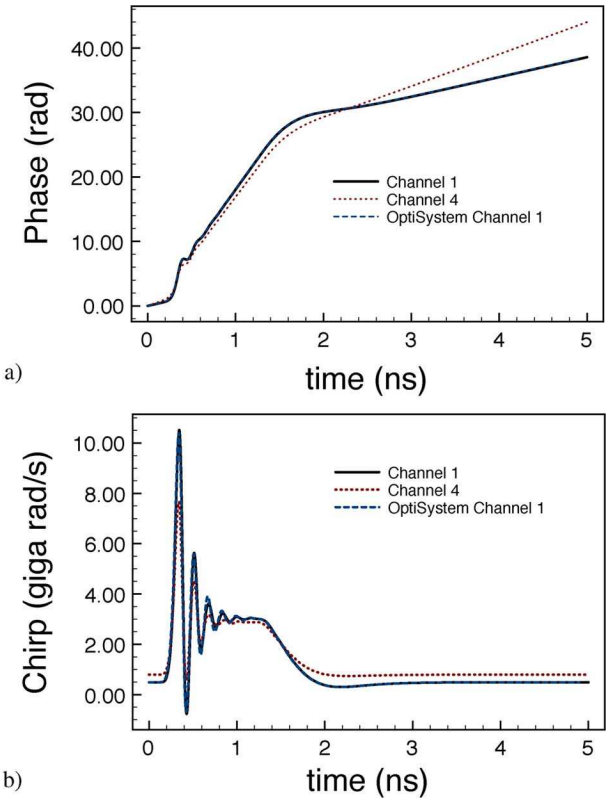

Fig. 19. Coarse WDM example. Transient plots for channels 1 and 4: (a) Optical phase and (b) Laser chirp.

model in *OptiSystem*; which then provided an optical signal for an *OptiSystem* simulation of the optical link. In the plots of optical power, phase and chirp (Fig. 18(b) and Fig. 19) it can be seen that *OptiSPICE* matches the *OptiSystem* results accurately. Modeling the whole system using *Spice* and *OptiSystem*, although doable, would be cumbersome due to the need to provide a convergence between the thermal coupling (which is nonlinear), the laser rate equations and the electrical simulation of all eight drivers and laser diodes.

D. PID Controller Example

The final example (see Fig. 20) shows a tightly coupled optoelectronic circuit—with feedback control on the optical output. This circuit consists of an optical link from source to detector; however, in this case the CW optical output is modulated externally by an electrooptic modulator. The optical signal provided by the laser is desired to be as independent of external phenomena as possible. To achieve this a proportional-integral-derivative (PID) controller is used. A small percentage of the optical power is split off from the output of the laser and is fed to a photodetector. The output from this detector is used as the input to a closed loop PID controller that adjusts the bias of the laser driver so as to keep the output power at a set-point.

Typically, the external disturbance would be in the form of a change in the ambient temperature. The feedback loop would adjust the bias voltage accordingly to compensate for the temperature change and keep the laser power constant. This circuit has two extremely different time scales. The thermal behavior of the device and the response of the PID controller are characterized by time constants in the microseconds or even milliseconds. On the other hand the data pulses in the system are typically in nanoseconds.

The plots in Fig. 21 show the operation of the PID feedback control. The temperature of the laser and bias circuitry was determined by a thermal subcircuit driven by a time dependent source representing an externally fluctuating substrate temperature. This temperature variation is shown in Fig. 21(a). The response of the laser output power is presented in Fig. 21(b). Responses for two cases are shown—open and closed loop cases. As expected, closing the PID feedback loop causes the laser bias to be adjusted to compensate for the temperature changes.

A second set of plots presented in Fig. 22 show the response of this circuit over a much smaller time scale. In this figure, the temperature of the circuit is essentially constant, however, a pseudo-random bit stream is used to bias the electrooptic modulator. The voltage input to the modulator is shown in Fig. 22(a) with 15 bits. The output power of the modulator can be seen in Fig. 22(b) showing the complex pulse shape produced by the nonlinearity of the modulator and the ringing behaviour in the voltage input due to lead inductance and capacitance. Finally, Fig. 22(c) presents the chirp (determined from the phase of the output) introduced in the optical signal by the modulator. It is important to model modulator chirp and in this case, it can be

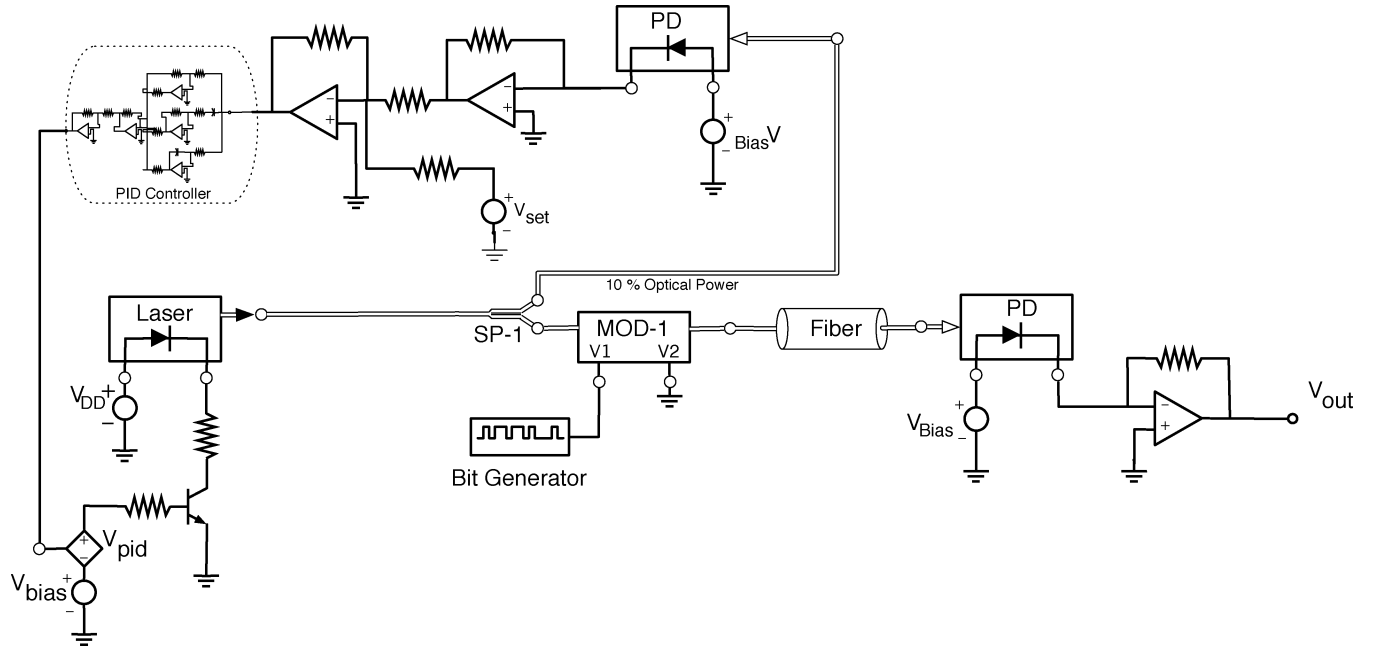

Fig. 20. Schematic for optical link with power monitor and temperature control.

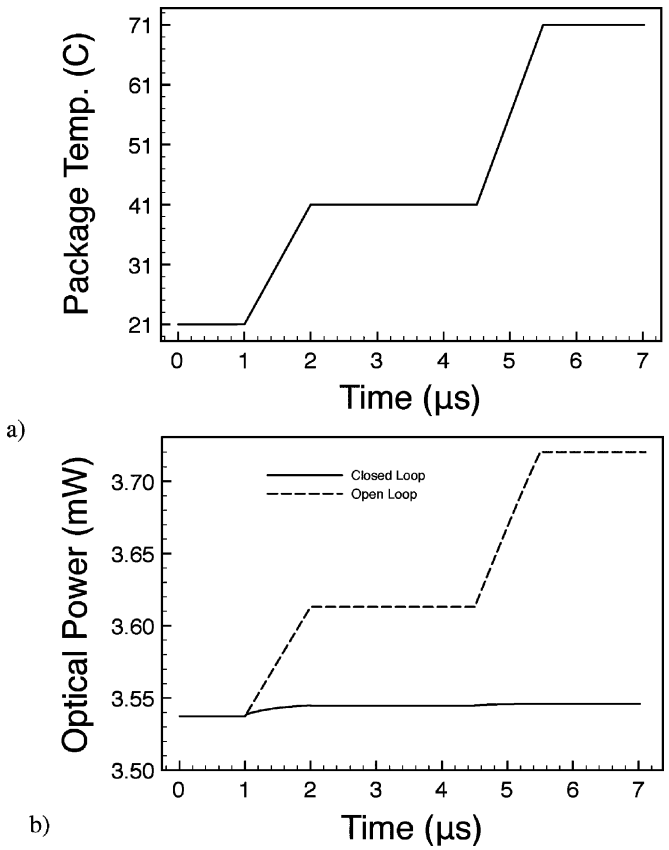

Fig. 21. Optical link with temperature controller example. (a) Package Temperature. (b) Laser optical power output (open and closed loop).

seen clearly. The laser has a constant chirp close to 3×10^9 Radians/s; and it can be seen that the modulator introduces a substantial variation in the chirp as the input signal switches from one value to the other.

Comparing results for this circuit with *SPICE* and *OptiSystem* proved to be difficult due to the feedback present in the system. The electronic pieces of the circuit were tested individually and comparison with *SPICE* showed a very good agreement. The optical portions of the circuit were compared to *OptiSystem* results and once again a very close comparison was obtained. A few manual iterations of the entire circuit were undertaken and convergence proved to be slow and cumbersome.

VI. Conclusion

As the integration of electrical and optical components becomes increasingly common at board, package and chip levels there will be a pronounced need for a self-consistent opto-electronic CAD environment. This paper presents a framework for implementing such a simulation environment for mixed electrical and optical circuits and systems using an MNA formulation. In particular, an optical node is formulated which includes the magnitude and phase of the optical signal being simulated, the choice of these state variables is crucial for efficient simulation. The optical signal is comprised of two propagating complex envelopes one in the forward direction and the other in the reverse direction. This formulation allows for the simulation of a large number of optical effects including mode matching across optical interfaces, the use of multiple optical channels and optical interference.

The paper presents models for a variety of devices. These include sources, detectors, multimode fiber and interference based devices. In the final section, the method is illustrated with a number of examples including a multimode fiber optical link, a integrated array of laser sources and a feedback controlled laser modulated laser source. For the simpler circuits *OptiSPICE* results are compared to commercial simulators where appropriate and found to agree closely. Effects illustrated include the ability to simulate circuits with very short

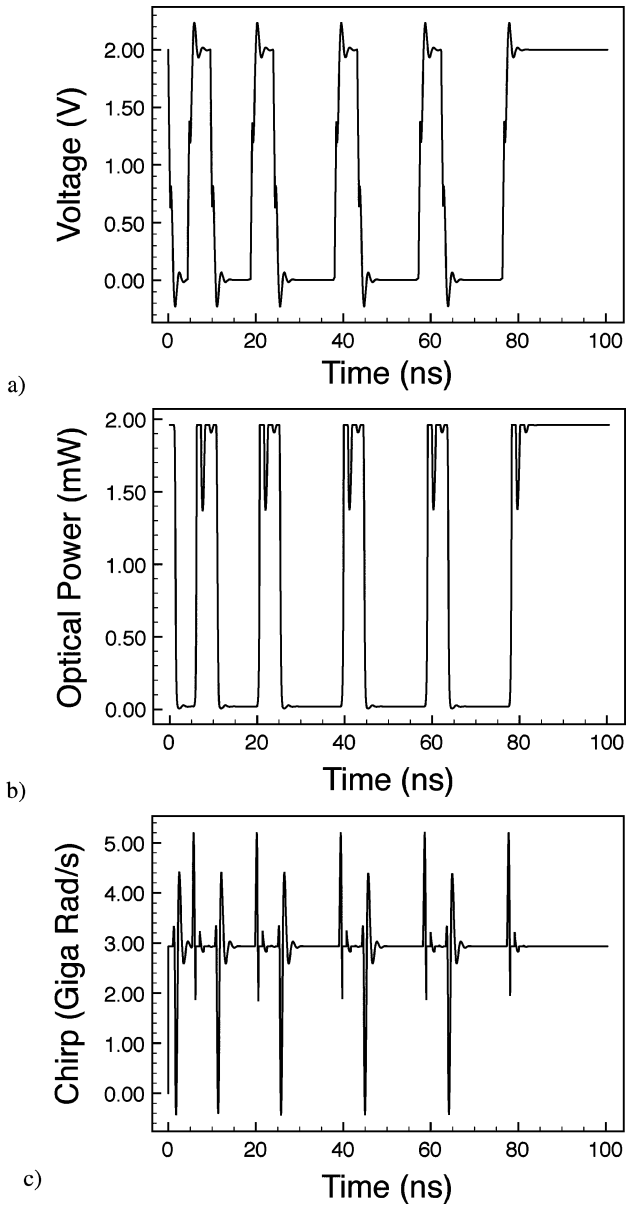

Fig. 22. Optical link with temperature controller example. Modulation results using an Electro-Absorption Modulator. (a) Input voltage. (b) Optical output power. (c) Optical output chirp.

pulses and significant fiber optical delays, pulse reflection and interference, thermal effects, and self-consistent simulation encompassing the electrical, thermal, and optical domains.

REFERENCES

[1] R. Nagarajan, C. Joyner, J. Schneider, R. P. , J. Bostak, T. Butrie, A. Dentai, V. Dominic, P. Evans, M. Kato, M. Kauffman, D. Lambert, S. Mathis, A. Mathur, R. Miles, M. Mitchell, M. Missey, S. Murthy, A. Nilsson, F. Peters, S. Pennypacker, J. Pleumeekers, R. Salvatore, R. Schlenker, R. Taylor, H.-S. Tsai, M. Van Leeuwen, J. Webjorn, M. Ziari, D. Perkins, J. Singh, S. Grubb, M. Reffle, D. Mehuys, F. Kish, and D. Welch, "Large-scale photonic integrated circuits," *IEEE Trans. Sel. Topics Quantum Electron.*, vol. 11, no. 1, pp. 50–65, Jan.–Feb. 2005.

[2] Z. Mi, J. Yang, P. Bhattacharya, G. Qin, and Z. Ma, "High-performance quantum dot lasers and integrated optoelectronics on si," *Proc. IEEE*, vol. 97, no. 7, pp. 1239–1249, Jul. 2009.

[3] Z. Yuan, A. Anopchenko, N. Daldosso, R. Guider, D. Navarro-Urrios, A. Pitanti, R. Spano, and L. Pavesi, "Silicon nanocrystals as an enabling material for silicon photonics," *Proc. IEEE*, vol. 97, no. 7, pp. 1250–1268, Jul. 2009.

[4] J. Leuthold, W. Freude, J.-M. Brosi, R. Baets, P. Dumon, I. Biaggio, M. Scimeca, F. Diederich, B. Frank, and C. Koos, "Silicon organic hybrid technology platform for practical nonlinear optics," *Proc. IEEE*, vol. 97, no. 7, pp. 1304–1316, Jul. 2009.

[5] K. Ohashi, K. Nishi, T. Shimizu, M. Nakada, J. Fujikata, J. Ushida, S. Torii, K. Nose, M. Mizuno, H. Yukawa, M. Kinoshita, N. Suzuki, A. Gomyo, T. Ishi, D. Okamoto, K. Furue, T. Ueno, T. Tsuchizawa, T. Watanabe, K. Yamada, S.-I. Itabashi, and J. Akedo, "On-chip optical interconnect," *Proc. IEEE*, vol. 97, no. 7, pp. 1186–1198, Jul. 2009.

[6] R. Tummala, "Sop: What is it and why? A new microsystem-integration technology paradigm-Moore's law for system integration of miniaturized convergent systems of the next decade," *IEEE Trans. Adv. Packag.*, vol. 27, no. 2, pp. 241–249, May 2004.

[7] M. Iyer, P. Ramana, K. Sudharsanam, C. Leo, M. Sivakumar, B. L. S. Pong, and X. Ling, "Design and development of optoelectronic mixed signal system-on-package (sop)," *IEEE Trans. Adv. Packag.*, vol. 27, no. 2, pp. 278–285, May 2004.

[8] J. Minz, S. Thyagara, and S. K. Lim, "Optical routing for 3-d system-on-package," *IEEE Trans. Compon. Packag. Technol.*, vol. 30, no. 4, pp. 805–812, Dec. 2007.

[9] G.-K. Chang, D. Guidotti, F. Liu, Y.-J. Chang, Z. Huang, V. Sundaram, D. Balaraman, S. Hegde, and R. Tummala, "Chip-to-chip optoelectronics sop on organic boards or packages," *IEEE Trans. Adv. Packag.*, vol. 27, no. 2, pp. 386–397, May 2004.

[10] R. Soref, "Silicon-based optoelectronics," *Proc. IEEE*, vol. 81, no. 12, pp. 1687–1706, Dec. 1993.

[11] R. Soref, "The past, present, and future of silicon photonics," *IEEE Trans. Sel. Topics Quantum Electron.*, vol. 12, no. 6, pp. 1678–1687, Nov.–Dec. 2006.

[12] L. Tsybeskov, D. Lockwood, and M. Ichikawa, "Silicon photonics: CMOS going optical," *Proc. IEEE*, vol. 97, no. 7, pp. 1161–1165, Jul. 2009.

[13] K. Wada, S. Park, and Y. Ishikawa, "Si photonics and fiber to the home," *Proc. IEEE*, vol. 97, no. 7, pp. 1329–1336, Jul. 2009.

[14] A. Krishnamoorthy, R. Ho, X. Zheng, H. Schwetman, J. Lexau, P. Koka, G. Li, I. Shubin, and J. Cunningham, "Computer systems based on silicon photonic interconnects," *Proc. IEEE*, vol. 97, no. 7, pp. 1337–1361, Jul. 2009.

[15] G. Agrawal, *Fiber-Optic Communication Systems*. New York: Wiley , 2003.

[16] C. DeCusatis, *Fiber Optic Data Communication*. New York: Elsevier, 2008.

[17] M. Neifeld and W. Chou, "Spice-based optoelectronic system simulation," *Appl. Opt.*, vol. 37, no. 26, pp. 6093–6104, 1998.

[18] S. Ozyazici and N. Dogru, "Ultrashort pulse generation by spice simulation of gain switching in quantum well laser," in *Conf. Lasers Electro-Optics—Pacific Rim, 2007 (CLEO/Pacific Rim 2007)*, Aug. 2007, pp. 1–2.

[19] S.-W. Lee, E.-C. Choi, and W.-Y. Choi, "Optical interconnection system analysis using spice," in *Pacific Rim Conf. Lasers and Electro-Optics, 1999 (CLEO/Pacific Rim'99)*, 1999, vol. 2, pp. 391–392, vol. 2.

[20] B. Whitlock, J. Morikuni, E. Conforti, and S.-M. Kang, "Simulation and modeling: Simulating optical interconnects," *IEEE Circuits Devices Mag.*, vol. 11, no. 3, pp. 12–18, May 1995.

[21] A. Yang and S. Kang, "ismile: A novel circuit simulation program with emphasis on new device model development," in *Proc. 26th Conf. Design Automat.*, Jun. 1989, pp. 630–633.

[22] S. Levitan, T. Kurzweg, P. Marchand, M. Rempel, D. Chiarulli, J. Martinez, J. Bridgen, C. Fan, and F. McCormick, "Chatoyant: A computer-aided design tool for free-space optoelectronic systems," *Appl. Opt.*, vol. 37, no. 26, pp. 6078–6092, Sep. 1998.

[23] M. Kahrs, S. Levitan, D. Chiarulli, T. Kurzweg, J. Martinez, J. Boles, A. Davare, E. Jackson, C. Windish, F. Kiamilev, A. Bhaduri, M. Taufik, X. Wang, A. Morris, J. Kruchowski, and B. Gilbert, "System-level modeling and simulation of the 10 g optoelectronic interconnect," *J. Lightwave Technol.*, vol. 21, no. 12, pp. 3244–3256, Dec. 2003.

[24] J. Eker, J. Janneck, E. Lee, J. Liu, X. Liu, J. Ludvig, S. Neuendorffer, S. Sachs, and Y. Xiong, "Taming heterogeneity—The ptolemy approach," *Proc. IEEE*, vol. 91, no. 1, pp. 127–144, Jan. 2003.

[25] T. Quarles, A. Newton, D. Pederson, and A. Sangiovanni-Vincentelli, SPICE 3 Version 3F5 User's Manual Dept. EECE, Univ. California, Berkeley.

[26] C. Ho, A. Ruehli, and P. Brennan, "The modified nodal approach to network analysis," *Trans. on Circuits and Systems*, vol. 22, pp. 504–509, Jun. 1975.
[27] J. D. Jackson, *Classical Electrodynamics*. New York: Academic, Aug. 1998, 2009, vol. 2009, no. 12.
[28] T. Tamir, *Guided-Wave Optoelectronics*. Berlin, Germany: Springer=Verlag, 1995.
[29] P. Pepeljugoski, S. E. Golowich, A. J. Ritger, P. Kolesar, and A. Risteski, "Modeling and simulation of next-generation multimode fiber links," *J. Lightwave Technol.*, vol. 21, pp. 1242–1255, May 2003.
[30] N. Cheng and J. Cartledge, "Measurement-based model for mqw electroabsorption modulators," *J. Lightwave Technol.*, vol. 23, no. 12, pp. 4265–4269, Dec. 2005.
[31] J. C. Cartledge and R. C. Srinivasan, "Extraction of dfb laser rate equation parameters for system simulation purposes," *J. Lightwave Technol.*, vol. 15, no. 5, pp. 852–860, Mar. 1997.
[32] P. V. Mena, J. J. Morikuni, S. M. Kang, A. V. Harton, and K. W. Wyatt, "A simple rate-equation-based thermal vcsel model," *J. Lightwave Technol.*, vol. 17, no. 5, pp. 865–872, May 1999.
[33] J. Campbell, B. Johnson, G. Qua, and W. Tsang, "Frequency response of inp/ingaasp/ingaas avalanche photodiodes," *J. Lightwave Technol.*, vol. 7, no. 5, pp. 778–784, May 1989.
[34] C.-L. Chen, *Foundations for Guided-Wave Optics*. New York: Wiley, 2006.
[35] G. Keiser, *Optical Fiber Communications*. New York: McGraw-Hill, 2000.
[36] SPICE [Online]. Available: http://www.synopsys.com/Tools/Verification/AMSVerification/CircuitSimulation/HSPICE
[37] C. N. and J. C. Cartledge, "Measurement-based model for mqw electroabsorption modulators," *J. Lightwave Technol.*, vol. 23, no. 12, pp. 4165–4269, Dec. 2005.
[38] OptiSystem [Online]. Available: http://www.optiwave.com/products/system_overview.html

Pavan Gunupudi (S'97–M'02) received his B.Tech. degree from the Indian Institute of Technology, Chennai, India, in 1997, and the Ph.D. degree from Carleton University, Ottawa, ON, Canada, in 2002.

He then joined the Department of Electronics at Carleton University and is presently an Associate Professor. His research interests include signal integrity, high-speed VLSI systems, and multidisciplinary simulation. He has authored more than 40 journal and conference papers and is a co-author of OptiSPICE.

Tom Smy received the B.Sc. and Ph.D. degrees in electrical engineering from the University of Alberta, Edmonton, AB, Canada, in 1986 and 1990, respectively.

He is a Professor in the Department of Electronics at Carleton University, Ottawa, ON, Canada. His current research interests include optical, thermal and multiphysics simulation of electronic devices/packages and modules, the study and simulation of thin film growth and microstructures, and a variety of backend processing projects. He has published over 100 journal papers and is a co-author of the OptiSPICE, Atar, SIMBAD, and 3D-Films simulators.

Jackson Klein received the B.Sc. degree in electrical engineering from the Federal University of Santa Maria, Brazil, in 1993, and the M.Sc. and Ph.D. degrees in electrical engineering, in 1995 and 1999, respectively, from UNICAMP, Brazil, and the M.B.A. degree from the University of Ottawa, ON, Canada.

He has been working with design and development of computer-aided design and analysis tools for optical communication systems for more than 15 years. He joined Optiwave after receiving the Ph.D. and since 1999 he has been part of the Research and Development Group at Optiwave Corporation as the Director of Optical Systems and one of the main researchers and designers of OptiSystem and OptiSPICE technologies. He is the author of over 25 conference papers and technical articles.

Z. Jan Jakubczyk received the M.Sc. degree in engineering physics from the Silesian Technical University, in 1976, and the Ph.D. degree from the Institute of Fundamental Research, Warsaw, Poland, in 1984, and the MBA degree from the University of Ottawa, Canada, in 2004.

From 1976 to 1986 he was an Associate Professor at the Silesian Technical University. From 1986 to 1988 he was a Research Associate at Laval University, Quebec, Canada. From 1989 to 1994 he was a Research Scientist at the National Optics Institute in Quebec, Canada. His research activities included surface acoustic waves (SAW) applications and waveguide properties of photonic devices. In 1994, he founded Optiwave Corporation where he is the CEO.